Water Science & Technology

Water Science & Technology Vol 00 No 0, 1 doi: 10.2166/wst.2021.211

Magnetically attracted iron scrap anode based electrocoagulation for phosphate removal

Dandan Zhu[a,b], Xiaoting Hong[a,*] and K. S. Hui[c]

[a] Department of Chemistry, Zhejiang Sci-Tech University, Hangzhou 310018, China
[b] Xiangshan Branch of Ningbo Environmental Protection Bureau, Ningbo 315700, China
[c] School of Mathematics, Faculty of Science, University of East Anglia, Norwich, NR4 7TJ, United Kingdom
*Corresponding author. E-mail: hanren.xiaoting@gmail.com

XH, 0000-0002-2420-4257

ABSTRACT

This study shows the effectiveness of a novel electrocoagulation process using magnetically attracted iron scrap anodes for phosphate removal from aqueous solution. The effect of contact time, reaction temperature, dose of iron scrap, initial phosphate concentration, applied voltage, pH, magnetic force, and the species of competing anions on the efficiency of phosphate removal and the reaction products has been investigated. The techniques of XRD, XPS, and VSM were used to characterize the elemental composition and the types of the reaction products in order to clarify the interaction between novel anode and phosphate ions. The removal of phosphate was fitted by a pseudo first-order reaction kinetic model. The results showed that magnetically attracted iron scrap anodes was electrodissoluted under an applied potential and reacted with phosphate into Fe-hydroxo-phosphate complexes. The work suggested that electrocoagulation using magnetically attracted iron scrap anodes had the potential to become a promising technique for phosphate precipitation.

Key words: electrocoagulation, Fe-hydroxo-phosphate complexes, magnetically attracted iron scrap, phosphate removal

HIGHLIGHTS

- Electrocoagulation by magnetically attracted iron scrap was used for phosphate removal.
- The effect of different parameters on novel electrocoagulation was investigated.
- Elemental composition and the type of the reaction product were characterized XRD, XPS, and VSM.
- Fe-hydroxo-phosphate complexes were formed during iron scrap electrocoagulation.
- Iron scrap waste was used for high value electrode.

GRAPHICAL ABSTRACT

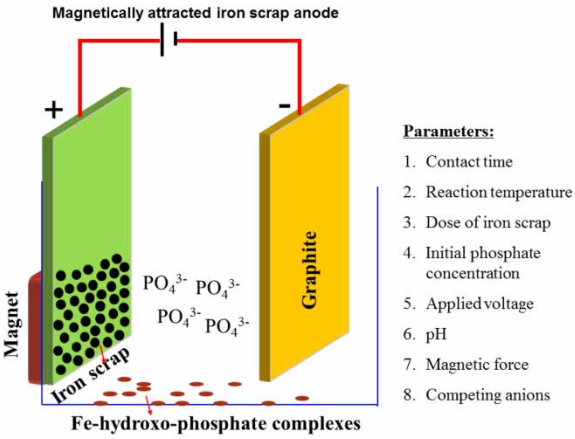

INTRODUCTION

Industrial wastewater and agricultural runoffs with excessive phosphorus directly or indirectly discharge into waterbody in terms of phosphate (PO_4^{3-}), hydrogen phosphate (HPO_4^{2-}) and dihydrogen phosphate (H_2PO^{4-})

(Fulazzaky *et al.* 2014). The excess dissolved phosphate is well recognized as a primary source of eutrophication, which leads to algae boom, opacity and oxygen depletion. Furthermore, natural phosphorus has significantly declined both in the quantity and the quality in the past decades (Lei *et al.* 2017). The potential shortage of phosphorus resources along with the over-discharge of phosphorus-containing wastewater have created an increased awareness of the importance of phosphorus recovery and recycling.

Thus, different technologies have been developed to mitigate phosphorus discharge to the environment including biological and chemical treatments (Sun *et al.* 2021). Struvite formation is regarded as one of the most promising chemical precipitation ways (González *et al.*). However, it relies on different Mg sources to assist struvite formation, which makes the process less economically attractive because of the low concentration of Mg^{2+} in wastewater (Barbosa *et al.* 2016). Alternatively, a novel process of electrochemical induced CaP precipitation on the cathode has been reported. Unfortunately, the phosphate removal efficiency of the process suffers CaP coverage on the cathode and a saturation of Ca and P (Lei *et al.* 2017). Electrolysis appears as a viable onsite sanitation solution for phosphate recovery from human waste, however, this strategy requires costly TiO_2-coated semiconductor anodes and suffers hydroxyapatite coverage on the cathode (Cid *et al.* 2018; Hou *et al.* 2021).

Electrocoagulation (EC), as a well-known electrochemical process, has received considerable attention for phosphorus precipitation due to its high feasibility and efficiency (Zeng *et al.*). Traditionally, zero-valent-iron (ZVI) plates were used as the electrode of electrocoagulation process. The reaction mechanisms of ferrous or ferric ions with phosphate were evaluated using both isotherm models and thermodynamic models (Vasudevan *et al.* 2008). Recently, a reverse-electric-field/air cathode electrocoagulation reactor was developed for high efficient phosphate removal from domestic wastewater compared to conventional electrocoagulation (Tian *et al.* 2017). A migration electric-field assisted electrocoagulation system was further developed to increase phosphate removal efficiency from domestic wastewater (Tian *et al.* 2018).

Unfortunately, electrocoagulation with ZVI plate inevitably suffers the passivation due to the formation of iron (oxyhydr)oxide passive layers on the surface of Fe(0) plates (Veluchamy *et al.* 2017; Samir Naje *et al.* 2019), resulting in a decrease in anodic interface potential favoring a larger faradaic current efficiency (Dubrawski *et al.* 2015). The dissolution and passivation rate of iron were experimentally verified to strongly depend on the electrode potential, ionic strength, ionic type, and the solution pH (Lorenz *et al.* 2002). Mechanical cleaning (Lakshmanan *et al.* 2009), the polarity of the electrodes (Timmes *et al.* 2010), and addition of halide salts (Adamovic *et al.* 2016) were reportedly the most efficient and reliable methods to clean the scale and fouling on the electrode for electrode maintenance.

ZVI particle has drawn great attention for the remediation of a wide variety of contaminants in groundwater and wastewater because of its high efficiency, low cost and nontoxic characteristics (Li *et al.* 2018; Jiang *et al.* 2020). Numerous researches reported on the phosphate removal from water by ZVI focusing on influence of different parameters such as solution composition (Eljamal *et al.* 2016), initial phosphate concentration ZVI aging (Sleiman *et al.* 2017), the enhancement of ZVI by different supporters (Khalil *et al.* 2017), and activation of persulfate by nanosized zero-valent iron (Zhao *et al.* 2016; Kim *et al.* 2018). Main focus of ZVI particle related research is how to further enhance the removal efficiency in many applications.

This work was motivated by the wide application of ZVI particle in environmental remediation and the disadvantages of ZVI plate electrocoagulation. Therefore, a novel electrocoagulation process using magnetically attracted iron scrap anodes was designed for phosphate removal. This system has several advantages: (1) economies of iron material because of low cost of iron scrap, (2) immobilization of iron scraps via magnetic field, (3) effectively avoid passivation compared to the iron plate anode because of higher reaction surface, (4) providing a promising method for reclamation of iron scraps, (5) no additional chemicals for this electrocoagulation, (6) no need to adjust the pH value of the solution. This work provides a promising approach for phosphate removal while this iron scrap anode could also be used for novel electro-Fenton process.

MATERIALS AND METHODS

Material

Chemicals used were analytical reagents of high purity. Ultrapure water with resistivity of 18.2 MΩ-cm from a Milli-Q(Millipore) water purification system was used for the experiments. Sodium nitrate ($NaNO_3$, 99%), sodium sulfate decahydrate (Na_2SO_4, 99%), nitric acid (HNO_3, 65–68%), sulfate acid (H_2SO_4, 98%), sodium hydroxide (NaOH, 97%), and potassium dihydrogen phosphate (KH_2PO_4, 99%) were obtained from Aladdin

Chemistry Co., Ltd (Shanghai, China). Iron scraps (50–100 mech size) were collected from a manufacture in Hangzhou. Graphite flakes were supplied by Qingdao baofeng graphite Co., Ltd.

Analytical techniques

All samples were filtered through 0.22 μm pore diameter syringe filters (polyvinylidenedifluoride, PVDF, 25 mm diameter, Restek Corporation) and analyzed for phosphate using ammonium molybdate spectrophotometric method by continuous flow analyzer (model AA3, SEAL, Germany). Removal rate was calculated based on initial and final concentrations. A pH probe (SevenMulti, Mettler-Toledo International Inc.) and conductometer (Rex Chemical Corp, Shanghai) were used to measure solution pH and conductivities. X-ray diffraction (XRD) patterns were recorded with a Bruker D8 advance diffractometer with monochromatic Cu Kα irradiation in the 2θ angular regions between 10 and 90°. XPS spectra were obtained on a Thermo Fisher Scientific ESCALAB 250Xi XPS spectrometer using Al Kα (1,486.6 eV) as the radiation source. The binding energy was calibrated by means of the peak energy of C 1s at 284.5 eV (Gao *et al.* 2011), and the elemental compositions were determined from peak area ratios after the correction for the sensitivity factor for each element. A vibrating-sample magnetometer (VSM, USA) is a scientific instrument that measures magnetic properties.

Batch electrocoagulation using magnetically attracted iron scrap

Electrocoagulation using magnetically attracted iron scrap anodes were carried out in batch-scale reactor consisted of a 200 mL electrolyte glass tank. The sacrificial anode was 0.2 g iron scraps evenly distributed in a groove (40 mm × 25 mm × 2 mm) on the graphite surface (100 mm × 30 mm × 5 mm). These iron scraps were magnetically attracted by a magnet (40 mm × 20 mm × 5 mm, surface magnetic field strength ~ 2,004 gauss) outside of the glass tank. The cathode was a 100 mm × 25 mm × 1 mm graphite sheet. The interelectrode gap is 10 mm. The applied potential was provided by a PS325DII power supply (0–32 V, 0–5 A, Shenzhen Lodestar precision tools Co., Ltd). The solution pH was varied from acidic to neutral and alkaline (4.0, 5.0, 7.0, 8.0, and 10.0). The initial phosphate concentration ranged from 100 to 2,500 mg·L^{-1}. All experiments were carried out under constant voltage conditions. A series voltages of 1.2, 5.0, 10.0, 15.0 V were applied for the new type EC. For each sampling event, a volume of suspension was drawn from the reactor at 0, 5, 15, 30, 60, 120, and180 min, and then filtered through a 0.22 μm PVDF membrane for analysis.

RESULTS AND DISCUSSION

Figure 1(a) illustrates the effect of initial phosphate concentration from 100 to 2,500 mg·L^{-1} (pH values from 5.18 to 4.70) on the phosphate concentration remaining in the solution. It can be obtained that removal rates are 100.00%, 80.05%, 76.13%, 73.41%, and 53.60% for phosphate solutions from 100 mg·L^{-1} to 2,500 mg·L^{-1}. Obviously, an increase in concentration at a constant potential of 10 V and 0.2 g iron scrap result in decrease in removal efficiency because of limited iron amount although higher concentration solution has larger current density. The amount of as-formed iron hydroxides was insufficient to coagulate the higher amount of phosphate at higher phosphate concentration.

It is well-known that applied potential dramatically influence the phosphate precipitation efficiency of the iron electrocoagulation. The effect of applied potential on the phosphate removal was shown in Figure 1(b). As expected, the removal efficiency increased significantly with the increase in applied potential within 3 h because of higher coagulant dosage rate, bubble production rate, and size and floc growth rate at larger current density. The highest electrical potential of 15 V produced the highest phosphate precipitation rate of 93.89% and the negligible phosphate removal efficiency of 1.30% occurred in the lowest electrical potential of 1.2 V. When the results were fitted by first-order reaction, the first-order kinetic rate constant decreased from 79.02 min^{-1} at 15 V to 182.62 min^{-1} at 5 V. This is ascribed to the fact that at higher voltage the amount of iron oxidized increased, resulting in a greater amount of precipitate for the removal of phosphate.

Many researchers reported that there is an influence of the magnetic field on the rate of various chemical and electrochemical reactions of non-electrochemical dissolution of iron (Bech-Nielsen & Jaskuła 2008). Figure 1(c) is shown that the influence of gauss surface strength of magnet on the phosphate precipitation at applied potential of 10 V. Each magnet has 2004 gauss surface strength. The phosphate rates are 80.28% and 76.13% when five magnets and one magnet are used, respectively. It could be concluded from Figure 1(c) that the strength of magnetic field has slightly impact on the phosphate precipitation. Due to the ferromagnetic property of ZVI, its external the Lorentz force and magnetic gradient force have been proposed to contribute to the enhancement

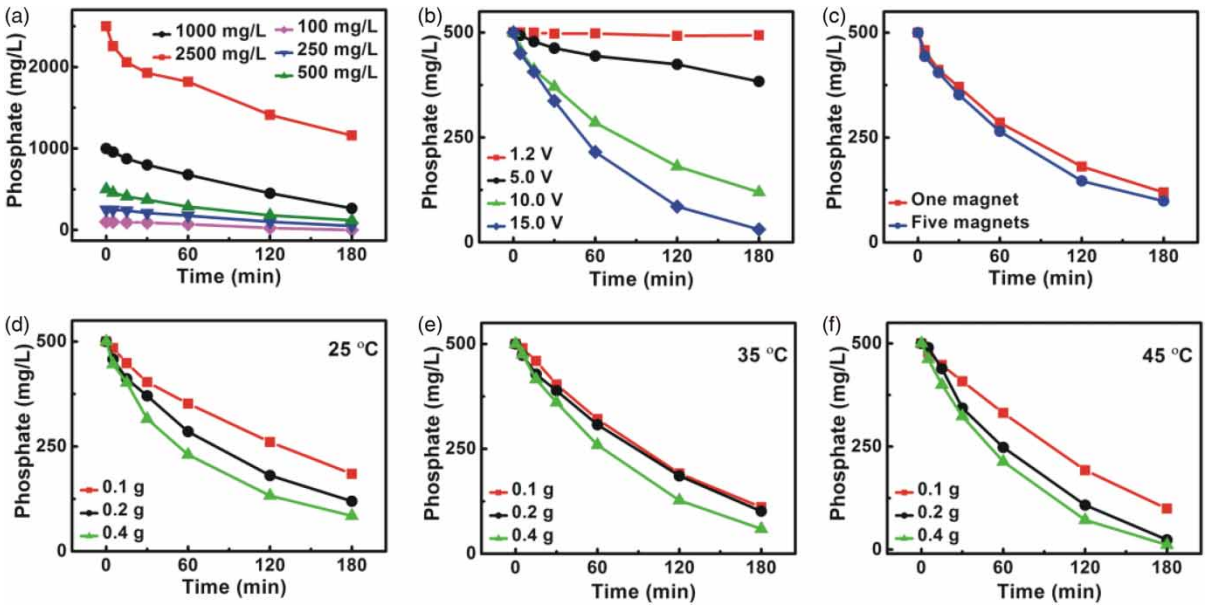

Figure 1 | Phosphate removal using magnetically attracted iron scrap electrocoagulation. Effect of (a) initial phosphate concentrations (10 V, 0.2 g ZVI), (b) applied potentials, and (c) magnetic forces on the phosphate removal at 25 °C; (d), (e) and (f) Effect of reaction temperature and the amount of iron scrap on phosphate removal.

in the reactivity and depassivation of ZVI (Xu *et al.* 2016). However, the effect of electric field is much greater than that of magnetic field because electrocoagulation is dominated by the applied potential in this case.

Figure 1(d)–1(f) depict the effect of various solution temperature from 25 to 45 °C and the amount of loaded iron scraps on the electrocoagulation performance. It can be observed that a higher amount of loaded iron scrap results in a greater amount of precipitate for the removal of phosphate due to a larger amount of iron oxidized at each temperature. Moreover, an increase in temperature causes an increase in removal efficiency. This may be attributed to the temperature-induced increase in the mass transferred of Fe^{2+} from the anode surface to the solution bulk and the increase of the rate of Fe^{2+} hydrolized to $Fe(OH)_2$ and reacted with PO_4^{3-} to form iron-phosphorus compound. These trends were confirmed by the first-order kinetic rate constants summarized in Table 1. The first-order kinetic rate increases with an increase in solution temperature and the amount of loaded iron scrap.

The electrocoagulation was carried out using magnetically attracted iron scrap under nitrogen aeration. Dissolution of the iron scrap anode leads to iron ions which react with phosphate ions and hydroxo ions. Fe-hydroxo-phosphate complexes was formed according to the following reactions of $xFe^{2+} + PO_4^{3-} + (2x-3)OH^- =$

Table 1 | The first-order kinetic parameters of phosphate removal by magnetically attracted iron scrap electrocoagulation

		First-order kinetic parameters		
		k_1 (min^{-1})	A_1 ($mg{\cdot}L^{-1}$)	R^2
25 °C	0.4 g Fe	60.49	421.75	0.996
	0.2 g Fe	90.71	423.21	0.995
	0.1 g Fe	143.77	428.89	0.995
35 °C	0.4 g Fe	80.21	487.80	0.999
	0.2 g Fe	140.57	539.42	0.998
	0.1 g Fe	154.31	576.64	0.999
45 °C	0.4 g Fe	83.83	544.11	0.999
	0.2 g Fe	157.09	678.05	0.997
	0.1 g Fe	223.44	722.77	0.999

$Fe_xPO_4(OH)_{(2x-3)(s)}$. XRD analysis of the ZVI samples was done to investigate the composition of the material. XRD patterns of iron scraps and preciptitate samples are shown in Figure 2. The peaks at 44.75° and 65.2° represented the characteristic peaks of ZVI correlated to lattice planes of (110) and (200) (Figure 2(a)). The XRD patterns from preciptitate samples showed a typical vivianite phase ($Fe_3(PO_4)_2{\cdot}8H_2O$) with a diffraction peak at 13.1 ° correlated to lattice planes of (020) (Figure 2(b)). However, the XRD reflexes characteristic for $Fe(OH)_2{\cdot}nH_2O$ could not be identified from bulk preciptitate samples due to its small amount of amorphous phase.

The vivianite mineral has been experimentally well studied and can be found in coatings of water pipes, soils, morasses, and sediments. Vivianite has paramagnetic properties as ambient temperature is higher than Neél temperature T_N (~10 K) (Pinto *et al.* 2014). Vivianite can disintegrate into strongly magnetic magnetite and weakly magnetic hematite upon heating in air through auto-oxidation or by the air when Fe^{2+} is oxidized to Fe^{3+}. The magnetic properties of the vivianite were investigated using VSM analysis at room temperature, on the magnetic field range from −1,000 to 1,000 mT. Magnetic hysteresis measurements showed that vivianite is of paramagnetic properties (Figure 3(a)). The saturation magnetization (*Ms*) and remanence (*Mr*) of vivianite are 0.05 and 0.003 $Am^2{\cdot}kg^{-1}$, respectively. The sample has a coercitivity of 4.5 mT and saturation field is 75 mT. Magnetic hysteresis measurements showed that iron scraps contained is of ferrimagnetic material recognized by the opening of the hysteresis loops. The result from magnetic hysteresis measurements confirmed the formation of vivianite during electrocoagulation process by magnetically attracted iron scrap in phosphate solution.

The elemental compositions of ZVI under various experimental conditions and reaction products were investigated by XPS. The broad survey scans (now shown) reveal that the surface of unreacted ZVI is composed mainly

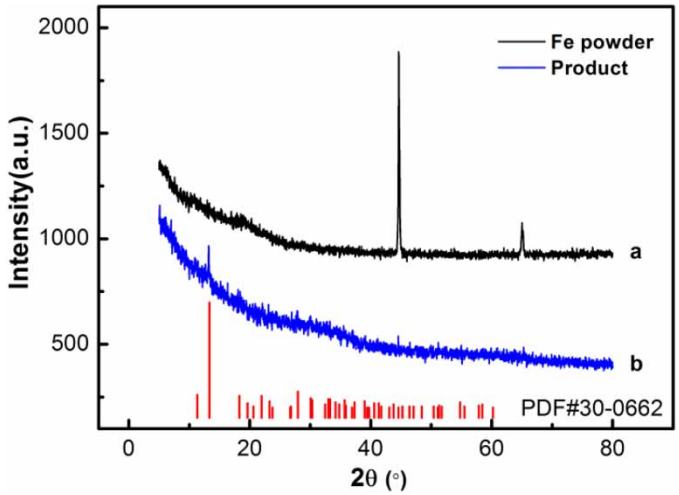

Figure 2 | XRD patterns of iron scraps and preciptitate samples.

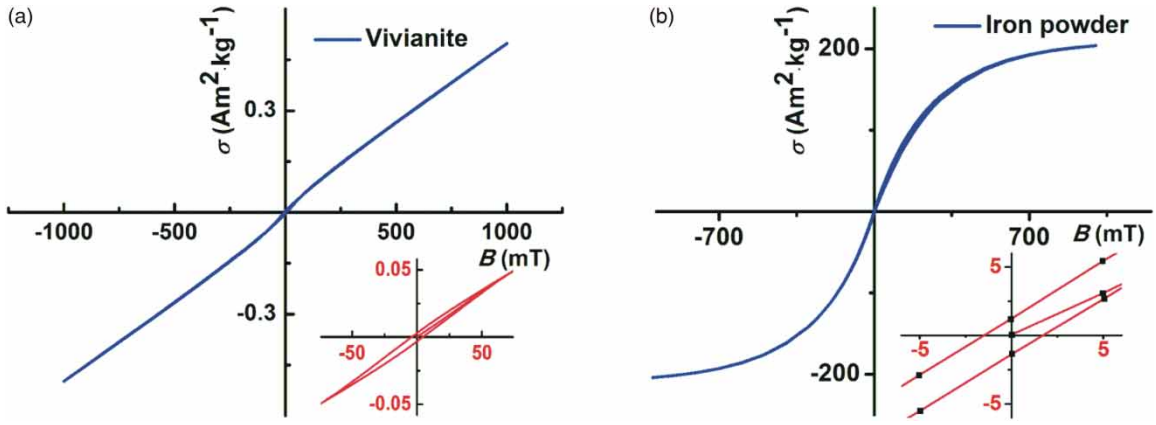

Figure 3 | Magnetic hysteresis measurements of vivianite and iron scraps by vibrating-sample magnetometer.

of Fe and O, and the surface of reacted ZVI and reaction product is composed of Fe, O, and P. The Fe 2p core level (Figure 4(a)) shows peaks of oxidized iron [Fe(III)] in the binding energies of Fe $2p_{1/2}$ (ca. 724.2 eV) and Fe $2p_{3/2}$ (ca. 710.6 eV), while the peaks at 718.8 eV represents the binding energies of shakeup satellite Fe $2p_{3/2}$ (Xu *et al.* 2016). Additionally, the small shoulder of Fe $2p_{3/2}$ (ca. 706.6 eV) suggests the presence of elemental iron (Fe^0) (Mondal *et al.* 2014). Thus, our results are in accordance with those reported in literature where the ZVI was shown to have a core-shell structure with an inner Fe^0 and an outer envelope of oxide layer. The Fe $2p_{3/2}$ spectrum indicated the presence of Fe(II) and Fe(III) on the reacted ZVI and precipitate reaction product (Figure 4(b) and 4(c)). No Fe^0 was detected on the reacted ZVI surfaces, indicating that the reacted ZVI surface was completely covered with a layer of reaction product (mainly iron phosphate). According to the peak-fitting results, the ratio of Fe(II)/Fe(III) on the surface of reacted ZVI (1.87) was higher than that on the surface of reaction product (1.05). The Fe 2p core level (Figure 4(b) and 4(c)) shows binding energy peaks of Fe(III) and Fe(II) are 725.2 eV and 711.3 eV, 722.9 eV and 709.3 eV for Fe $2p_{1/2}$ and Fe $2p_{3/2}$, respectively. The binding energies of Fe $2p_{1/2}$ and Fe $2p_{3/2}$ in Fe(III) shifted to higher values because of formation of Fe-hydroxo-phosphate complexes. The existence of Fe(II) is consistent with the ZVI coagulation process where Fe(II) ions were firstly generated. XPS result show the presence of this protective layer on the ZVI surface due to the fact that the penetration depth on surface of XPS (~nm) is much lower than that of XRD (~mm or μm). The P 2p XPS spectra of ZVI (1.2 V), ZVI (10 V), and reaction product were shown in Figure 4(d). No P was detected for iron scrap anodes at an applied potential of 1.2 V because of unmotivated electrocoagulation. Iron scrap anode (10 V) and reaction product show binding energy peaks of P 2p located at 133.5 eV. This result indicated the existence of phosphate complexes on the surface of the ZVI anode and reaction product.

Figure 5 shows the effect of competing anions of nitrate, sulfate, and acetate on phosphate removal by magnetically attracted iron scrap electrocoagulation with an applied potential of 10 V, phosphate concentration of 500 $mg{\cdot}L^{-1}$ and electrical conductivity of 850 $mS{\cdot}m^{-1}$. The reason why chloride ion has not been compared herein is that it will be oxidized to Cl_2 at an applied potential of 10 V. Figure 5(a)–5(c) represent that the rate of iron electro-coagulation at acidic and anoxic conditions is faster than that of the iron electro-coagulation by neutral and basic condition which is consistent with the result elsewhere (Huang & Zhang 2004). Nitrate, sulfate, and acetate have similar effect on phosphate removal (98–99%) at low pH of 4 and 5. As pH increases to near neutral (pH of 7 and 8), phosphate removal order follows SO_4^{2-} (99%, 96%) > NO_3^- (96%, 92%) > CH_3COO^-

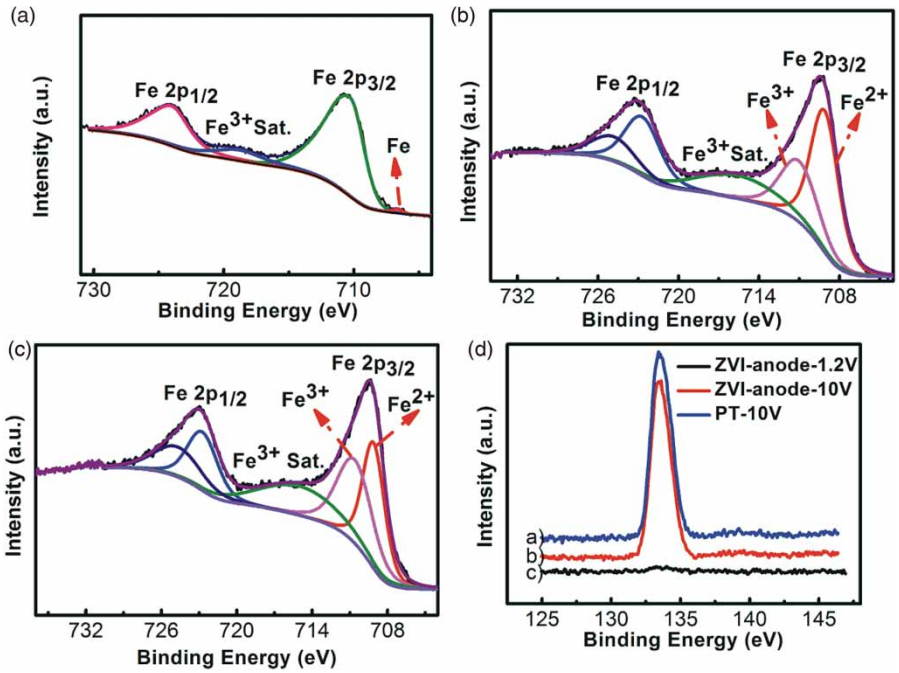

Figure 4 | XPS spectra of (a) ZVI at an applied potential of 1.2 V for 3 h, (b) ZVI at an applied potential of 10 V for 3 h, (c) reaction products collected at an applied potential of 10 V for 3 h, and (d) phosphate of ZVI (1.2 V), ZVI (10 V), and reaction product.

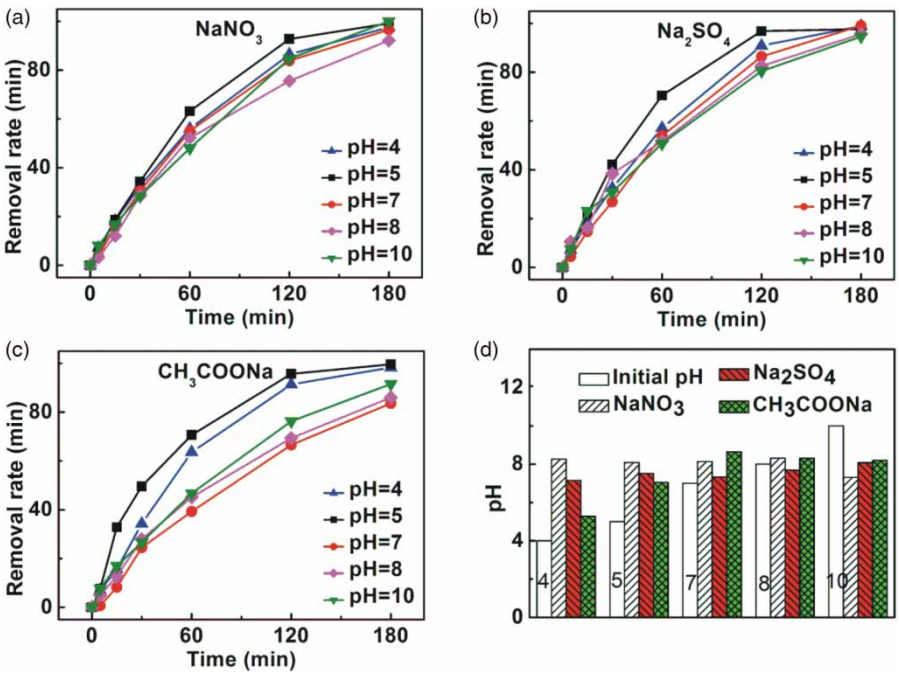

Figure 5 | Effect of competing anions (a) nitrate, (b) sulfate, and (c) acetate on phosphate removal by magnetically attracted iron scrap electrocoagulation with initial phosphate concentration of 500 mg·L^{-1}, 25 °C, and electrical conductivity of 850 mS·m^{-1} at different solution pH; (d) Initial and final pH value of the aqueous solution.

(84%, 86%). As pH further increases to high value of 10, phosphate removal order follows NO_3^- (100%) > SO_4^{2-} (95%) > CH_3COO^- (92%). Figure 5(d) shows the initial and final pH values of the aqueous solutions. Electrocoagulation at initial pH values of 4 and 5 results in pH increase where final pH values are 5 and 7, 7 and 8, 8 and 8 for solution containing acetate, sulfate, and nitrate, respectively. The final pH values maintained near neutral values of 7 and 8 at initial solution pH values of 7 and 8. The final pH values drop to 7, 8, and 8 for nitrate, sulfate, and acetate at initial pH values of 10. The overall pH change trends coincide with the report elsewhere (Bektaş *et al.* 2004).

CONCLUSIONS

In conclusion, a novel electrocoagulation process with magnetically attracted iron scrap anode was employed for phosphate removal. This process follows first-order kinetics and the phosphate removal rate increased significantly with the increase in applied potential (93.89% at 15 V, 1.30% at 1.2 V). The maximum and minimum values of removal rate are 100.00% and 53.60% when phosphate concentration are 100 mg·L^{-1} and 2,500 mg·L^{-1}. The effect of co-anions on phosphate removal follows the order of $SO_4^{2-} > NO_3^- > CH_3COO^-$ at pH < 10 and $NO_3^- > SO_4^{2-} > CH_3COO^-$ at pH < 10, respectively. The reaction preciptitate was Fe-hydroxo-phosphate complexes, mainly vivianite phase, $Fe_3(PO)_2{\cdot}8H_2O$. This iron scrap anode could easily be extended to novel electro-Fenton process and could also stimulate the reactions using other magnetic nanoparticle electrodes.

ACKNOWLEDGEMENTS

Financial supports for this work were provided by Natural Science Foundation of Zhejiang Province (LY18E080016), Open Foundation of State Environmental Protection Key Laboratory of Mineral Metallurgical Resources Utilization and Pollution Control (HB201909), and the Fundamental Research Funds of Zhejiang Sci-Tech University (2020Q048). Authors have full power to make these grants.

DATA AVAILABILITY STATEMENT

Data cannot be made publicly available; readers should contact the corresponding author for details.

REFERENCES

Adamovic, S., Prica, M., Dalmacija, B., Rapajic, S., Novakovic, D., Pavlovic, Z. & Maletic, S. 2016 Feasibility of electrocoagulation/flotation treatment of waste offset printing developer based on the response surface analysis. *Arabian Journal of Chemistry* **9**, 152–162.

Barbosa, S. G., Peixoto, L., Meulman, B., Alves, M. M. & Pereira, M. A. 2016 A design of experiments to assess phosphorous removal and crystal properties in struvite precipitation of source separated urine using different Mg sources. *Chemical Engineering Journal* **298**, 146–153.

Bech-Nielsen, G. & Jaskuła, M. 2008 The influence of a magnetic field on the non-electrochemical dissolution of iron. *Journal of Electroanalytical Chemistry* **624**, 327–328.

Bektaş, N., Akbulut, H., Inan, H. & Dimoglo, A. 2004 Removal of phosphate from aqueous solutions by electro-coagulation. *Journal of Hazardous Materials* **106**, 101–105.

Cid, C. A., Jasper, J. T. & Hoffmann, M. R. 2018 Phosphate recovery from human waste via the formation of hydroxyapatite during electrochemical wastewater treatment. *ACS Sustainable Chemistry & Engineering* **6**, 3135–3142.

Dubrawski, K. L., van Genuchten, C. M., Delaire, C., Amrose, S. E., Gadgil, A. J. & Mohseni, M. 2015 Production and transformation of mixed-valent nanoparticles generated by Fe(0) electrocoagulation. *Environmental Science & Technology* **49**, 2171–2179.

Eljamal, O., Khalil, A. M. E., Sugihara, Y. & Matsunaga, N. 2016 Phosphorus removal from aqueous solution by nanoscale zero valent iron in the presence of copper chloride. *Chemical Engineering Journal* **293**, 225–231.

Fulazzaky, M. A., Salim, N. A. A., Abdullah, N. H., Mohd Yusoff, A. R. & Paul, E. 2014 Precipitation of iron-hydroxy-phosphate of added ferric iron from domestic wastewater by an alternating aerobic–anoxic process. *Chemical Engineering Journal* **253**, 291–297.

Gao, Z., Wang, J., Li, Z., Yang, W., Wang, B., Hou, M., He, Y., Liu, Q., Mann, T., Yang, P., Zhang, M. & Liu, L. 2011 Graphene nanosheet/Ni^{2+}/Al^{3+} layered double-hydroxide composite as a novel electrode for a supercapacitor. *Chemistry of Materials* **23**, 3509–3516.

González, C., Fernández, B., Molina, F., Camargo-Valero, M. A. & Peláez, C. The determination of fertiliser quality of the formed struvite from a WWTP. *Water Science and Technology*. https://doi.org/10.2166/wst.2021.162.

Hou, C., Liu, H. & Li, Y. 2021 The preparation of three-dimensional flower-like TiO_2/$TiOF_2$ photocatalyst and its efficient degradation of tetracycline hydrochloride. *RSC Advances* **11**, 14957–14969.

Huang, Y. H. & Zhang, T. C. 2004 Effects of low pH on nitrate reduction by iron powder. *Water Research* **38**, 2631–2642.

Jiang, X., Lyu, S., Ali, M., Huang, J., Jiang, W., Qiu, Z. & Sui, Q. 2020 Enhancement of benzene degradation by persulfate oxidation: synergistic effect by nanoscale zero-valent iron (nZVI) and thermal activation. *Water Science and Technology* **82**, 998–1008.

Khalil, A. M. E., Eljamal, O., Amen, T. W. M., Sugihara, Y. & Matsunaga, N. 2017 Optimized nano-scale zero-valent iron supported on treated activated carbon for enhanced nitrate and phosphate removal from water. *Chemical Engineering Journal* **309**, 349–365.

Kim, C., Ahn, J.-Y., Kim, T. Y., Shin, W. S. & Hwang, I. 2018 Activation of persulfate by nanosized zero-valent iron (NZVI): mechanisms and transformation products of NZVI. *Environmental Science & Technology* **52**, 3625–3633.

Lakshmanan, D., Clifford, D. A. & Samanta, G. 2009 Ferrous and ferric ion generation during iron electrocoagulation. *Environmental Science & Technology* **43**, 3853–3859.

Lei, Y., Song, B., van der Weijden, R. D., Saakes, M. & Buisman, C. J. N. 2017 Electrochemical induced calcium phosphate precipitation: importance of local pH. *Environmental Science & Technology* **51**, 11156–11164.

Li, Y., Guo, X., Dong, H., Luo, X., Guan, X., Zhang, X. & Xia, X. 2018 Selenite removal from groundwater by zero-valent iron (ZVI) in combination with oxidants. *Chemical Engineering Journal* **345**, 432–440.

Lorenz, W. J., Staikov, G., Schindler, W. & Wiesbeck, W. 2002 The role of low-dimensional systems in electrochemical phase formation and dissolution processes. *Journal of The Electrochemical Society* **149**, K47–K59.

Mondal, P., Bhowmick, S., Jullok, N., Ye, W., Van Renterghem, W., Van den Berghe, S. & Van der Bruggen, B. 2014 Behavior of As(V) with ZVI–H_2O system and the reduction to As(0). *The Journal of Physical Chemistry C* **118**, 21614–21621.

Pinto, H. P., Michalkova, A. & Leszczynski, J. 2014 First-Principles studies of paramagnetic vivianite $Fe_3(PO_4)_2$•$8H_2O$ surfaces. *The Journal of Physical Chemistry C* **118**, 6110–6121.

Samir Naje, A., Ajeel, M. A., Mohamad Ali, I., Al-Zubaidi, H. A. M. & Alaba, P. A. 2019 Raw landfill leachate treatment using an electrocoagulation process with a novel rotating electrode reactor. *Water Science and Technology* **80**, 458–465.

Sleiman, N., Deluchat, V., Wazne, M., Mallet, M., Courtin-Nomade, A., Kazpard, V. & Baudu, M. 2017 Phosphate removal from aqueous solutions using zero valent iron (ZVI): influence of solution composition and ZVI aging. *Colloids and Surfaces A: Physicochemical and Engineering Aspects* **514**, 1–10.

Sun, S., Feng, C., Tong, S., Zhao, Y., Chen, N. & Zhu, M. 2021 Evaluation of advanced phosphorus removal from slaughterhouse wastewater using industrial waste-based adsorbents. *Water Science and Technology* **83**, 1407–1417.

Tian, Y., He, W., Zhu, X., Yang, W., Ren, N. & Logan, B. E. 2017 Improved electrocoagulation reactor for rapid removal of phosphate from wastewater. *ACS Sustainable Chemistry & Engineering* **5**, 67–71.

Tian, Y., He, W., Liang, D., Yang, W., Logan, B. E. & Ren, N. 2018 Effective phosphate removal for advanced water treatment using low energy, migration electric–field assisted electrocoagulation. *Water Research* **138**, 129–136.

Timmes, T. C., Kim, H.-C. & Dempsey, B. A. 2010 Electrocoagulation pretreatment of seawater prior to ultrafiltration: pilot-scale applications for military water purification systems. *Desalination* **250**, 6–13.

Vasudevan, S., Sozhan, G., Ravichandran, S., Jayaraj, J., Lakshmi, J. & Sheela, M. 2008 Studies on the removal of phosphate from drinking water by electrocoagulation process. *Industrial & Engineering Chemistry Research* **47**, 2018–2023.

Veluchamy, A., Sherwood, D., Emmanuel, B. & Cole, I. S. 2017 Critical review on the passive film formation and breakdown on iron electrode and the models for the mechanisms underlying passivity. *Journal of Electroanalytical Chemistry* **785**, 196–215.

Xu, H., Sun, Y., Li, J., Li, F. & Guan, X. 2016 Aging of zerovalent iron in synthetic groundwater: X-ray photoelectron spectroscopy depth profiling characterization and depassivation with uniform magnetic field. *Environmental Science & Technology* **50**, 8214–8222.

Zeng, J., Ji, M., Zhao, Y., Helmer, P. T. & Wang, H. Optimization of electrocoagulation process parameters for enhancing phosphate removal in a biofilm-electrocoagulation system. *Water Science and Technology*. https://doi.org/10.2166/wst.2021.132

Zhao, L., Ji, Y., Kong, D., Lu, J., Zhou, Q. & Yin, X. 2016 Simultaneous removal of bisphenol A and phosphate in zero-valent iron activated persulfate oxidation process. *Chemical Engineering Journal* **303**, 458–466.

Received 7 April 2021; accepted in revised form 22 May 2021. Available online 3 June 2021